The Journal of Experimental Biology 203, 1193–1200 (2000)
Printed in Great Britain © The Company of Biologists Limited 2000
JEB2366

THE AGEING OF THE LOW-FREQUENCY WATER DISTURBANCES CAUSED BY SWIMMING GOLDFISH AND ITS POSSIBLE RELEVANCE TO PREY DETECTION

WOLF HANKE[1,*], CHRISTOPH BRÜCKER[2] AND HORST BLECKMANN[1]

[1]*Institut für Zoologie der Rheinischen Friedrich-Wilhelms-Universität Bonn, Poppelsdorfer Schloß, D-53115 Bonn, Germany* and [2]*Aerodynamisches Institut der Rheinisch-Westfälischen Technischen Hochschule Aachen, Templergraben 55, D-52062 Aachen, Germany*

*e-mail: Bleckmann@uni-bonn.de

Accepted 24 January; published on WWW 9 March 2000

Summary

Wakes caused by swimming goldfish (*Carassius auratus*) were measured with a particle image velocimetry system and analyzed using a cross-correlation technique. Particle velocities in a horizontal plane (size of measuring plane 24 cm×32 cm or 20 cm×27 cm) were determined, and the vorticity in the plane was derived from these data. The wake behind a swimming goldfish can show a clear vortex structure for at least 30 s. Particle velocities significantly higher than background noise could still be detected 3 min after a fish (body length 10 cm) had passed through the measuring plane. Within this time span, the lateral spread of fish-generated wakes could exceed 30 cm for a 10 cm fish and 20 cm for a 6 cm fish. Measurements in a man-made open-air pond showed that water velocities in a quasi-natural still water environment can be as small as 1 mm s^{-1}. Background velocities did not exceed 3 mm s^{-1} as long as no moving animal was present in the measuring plane. The possible advantage for piscivorous predators of being able to detect and analyze fish-generated wakes is discussed.

Key words: lateral line, teleost, goldfish, *Carassius auratus*, hydrodynamics, particle image velocimetry, wake.

Introduction

Hydrodynamic receptor systems are well known from many aquatic and semiaquatic animals (for a review, see Bleckmann, 1994). They are used, for example, to detect predators, prey or conspecifics. Hydrodynamic receptor systems have been the subject of extensive morphological, physiological and behavioural investigations (e.g. Görner, 1963; Tautz and Sandeman, 1980; Budelmann and Bleckmann, 1988; Coombs and Janssen, 1989; Dehnhardt et al., 1998). However, despite recent advances in the investigation of hydrodynamic sensory systems, data on biologically relevant hydrodynamic stimuli, e.g. data on water disturbances caused by moving aquatic animals or by midwater animals performing certain behaviours, are still rare.

Animal-generated water movements can be measured using a laser Doppler anemometer (LDA) (e.g. Bleckmann et al., 1991) or a hot-wire anemometer (e.g. Kirk, 1985; Coombs et al., 1989). Both techniques have a high time resolution and are very sensitive (e.g. Blickhan et al., 1990, 1992; Bleckmann et al., 1991; Krick et al., 1997). However, they detect and measure water movements at a single point only. Moving aquatic animals produce flow fields whose spatial dimensions are often complex and thus may contain additional information relevant to other aquatic animals. Unfortunately, it is not possible to reconstruct the spatial aspects of a hydrodynamic flow field completely from single point measurements. To visualize directly the complex flow fields caused by animals, one can seed non-toxic dyes (e.g. Merzkirch, 1987) or neutrally buoyant particles (Vogel and Feder, 1966; Merzkirch, 1987) into the water. Rosen (1959) used a milk layer to visualize the spatial aspects of the water movements caused by a swimming fish. However, the study was performed in a narrow raceway which prevented the fish-generated water movements from spreading laterally. The stratified water method used by McCutchen (1977) to visualize fish-generated water movements also led to some useful observations. However, neither Rosen (1959) nor McCutchen (1977) measured fish-generated water movements for longer than 15 s. In addition, neither of the two studies yielded water velocity vector fields.

The most recent approach to measuring animal-generated water movements is particle image velocimetry (PIV) (Adrian, 1991). Using this technique, water movements of various scales can be investigated with a certain time resolution over a preselected space. The principle of PIV is to seed the water with neutrally buoyant particles, illuminate a thin layer of the seeded water with a suitable device and film or photograph the illuminated particles from a direction perpendicular to this layer. Using the PIV method, researchers have recently described the water disturbances surrounding aquatic invertebrates (Stamhuis and Videler, 1995) and those that can be measured for up to several seconds behind a swimming fish (Müller et al., 1997).

To date, no-one has attempted to measure fish-generated water

movements over a time span exceeding 15 s (in most cases, measurement periods are only 1 or 2 s), although swimming fish leave hydrodynamic tracks in the water that last much longer. Some piscivorous predators can use these hydrodynamic tracks to aid prey capture (G. Dehnhardt and B. Mauck, unpublished data). We have used a PIV system developed in our laboratory (Hanke and Bleckmann, 1997) to visualize and measure the water disturbances caused by swimming goldfish over a period of up to 5 min. Particle flow was analyzed using custom-designed software adapted to match the specific requirements of our experiments (Hanke and Brücker, 1998).

Materials and methods

Experimental animals

Two goldfish (*Carassius auratus* L., body length 6 and 10 cm) were trained to swim in a straight line through the middle of a water tank (100 cm×100 cm×50 cm, water level at least 40 cm; size of tank chosen to minimize wall effects) to reach a small compartment situated at the opposite wall, where they received a food reward. Before each measurement, the fish was kept in a small compartment at the start of the swimming route. Training consisted of conditioning the fish to a green flashing light (a bright light-emitting diode flashing at approximately 2 Hz). The flashing light was mounted at the lower end of a feeding tube that allowed the fish to be rewarded with a single mosquito larva.

Flow measurements

A custom-made PIV device was used to measure the flow in a horizontal plane (termed the measuring plane) around and behind a freely swimming goldfish. Data were analyzed by cross correlation of sequential frames in multiple time scales. The horizontal plane in which the flow was measured was

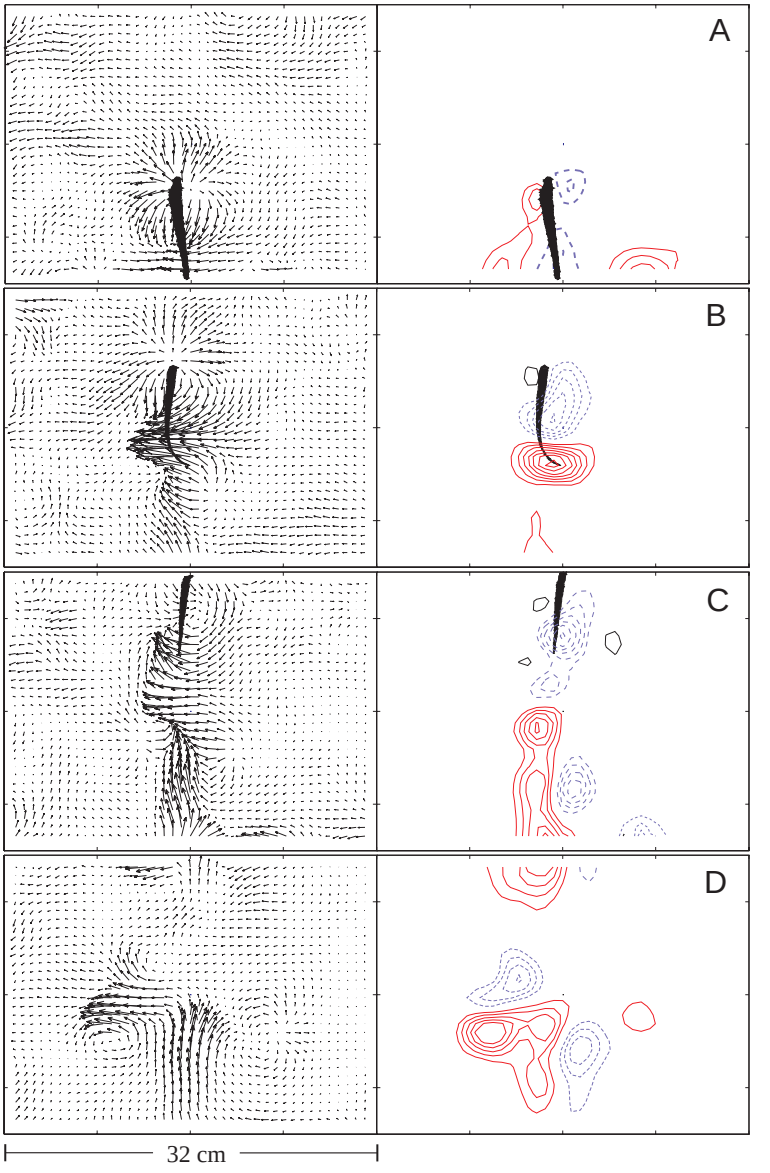

Fig. 1. Left: water velocities shown as vector fields in a typical trial (1) for t=0.6 s (A), 1.5 s (B), 2.3 s (C) and 7.8 s (D), where t=0 s is the time when the snout of the fish entered the field of view. Velocities are not to scale, for values see Fig. 3 and Table 1. The maximum velocity was at least 17 mm s^{-1}. Right: corresponding vorticities. Broken blue lines are contour lines for negative vorticity values, solid red lines indicate positive vorticity values. The difference between two successive contour lines is 0.02 s^{-1}. The time separation between frames used to calculate the values in Figs 1 and 2 was 0.04 s in the first 12 s, 0.2 s in the subsequent 48 s and 0.5 s after that.

illuminated with an array of 10 diode lasers (laser pointers, <5 mW each). The beam of each laser was passed through a glass rod which served as a cylinder lens and spread the beam in one direction, thus generating a light sheet approximately 1 mm thick. To visualize water movements, neutrally buoyant seeding particles (Vestosint 1101, donated by Hüls AG, Marl, Germany) were put into the water. Neither the illumination nor the particles harmed the fish.

Pictures were taken using two highly sensitive CCD camera modules (Conrad Electronic) mounted above the tank. One camera was mounted above the centre of the tank, the other camera was set up next to it to extend the field of view laterally up to the wall of the tank. The use of two cameras improved the spatial resolution and the use of light. The cameras were equipped with CCTV objectives with a fixed focal length of 8 mm and an aperture of f=1.2. Pictures were recorded using Panasonic NV-F70 HQ VCRs and digitized with a video-capture card (Miro Video DC30). The capture card supplies a hardware compression which was set to 1:10. This compression does not affect the quality of PIV results (Freek et al., 1997) and is sufficient to work at the speed of standard hard disk drives (data rate 1.9 Mbyte s^{-1} for 50 half-frames of 720 pixels×540 pixels).

Data analysis

The digitized pictures were stored on recordable compact discs and analyzed using a custom-designed correlation program. The range of water velocities that can occur in the wake of a fish is quite large. In principle, the velocity range of PIV depends on the adaptation of various parameters, the particle image diameter, the spatial resolution and the time scale (Adrian, 1997). While the time scale is usually fixed by the separation of the laser pulses, PIV with chronological time series recording offers the possibility of choosing different time periods between the correlation frames (multiple time scale processing). We used this method to improve the velocity range analyzed. A maximum time separation of 2 frames s^{-1} resulted in a correlation uncertainty below 0.1 mm s^{-1}, which was of the order of the background fluctuations in the tank after a 10 min settling time. Interrogation areas (the interrogation area is a section of the recorded frame that is subjected to the correlation procedure, see, for example, Keane and Adrian, 1992) were 64 pixels×64 pixels or 32 pixels×32 pixels depending on particle density, with an overlap of less than 50 %. Since our experiments were designed to investigate the long-term behaviour of the wake over its full width, the analysis procedure was not optimized regarding the velocity and vorticity resolution. The measurement of velocity and vorticity is biased towards zero because of the following effects.

First, seeding density was not always optimal as a result of experimental constraints. A seeding density of less than 12 particles per interrogation area biases the velocity measurement towards zero, partly because the rate of false vectors (‘outliers’) produced by the correlation procedure is enhanced, particularly for higher velocities (Host-Madsen and McCluskey, 1994). Outliers were removed as far as possible

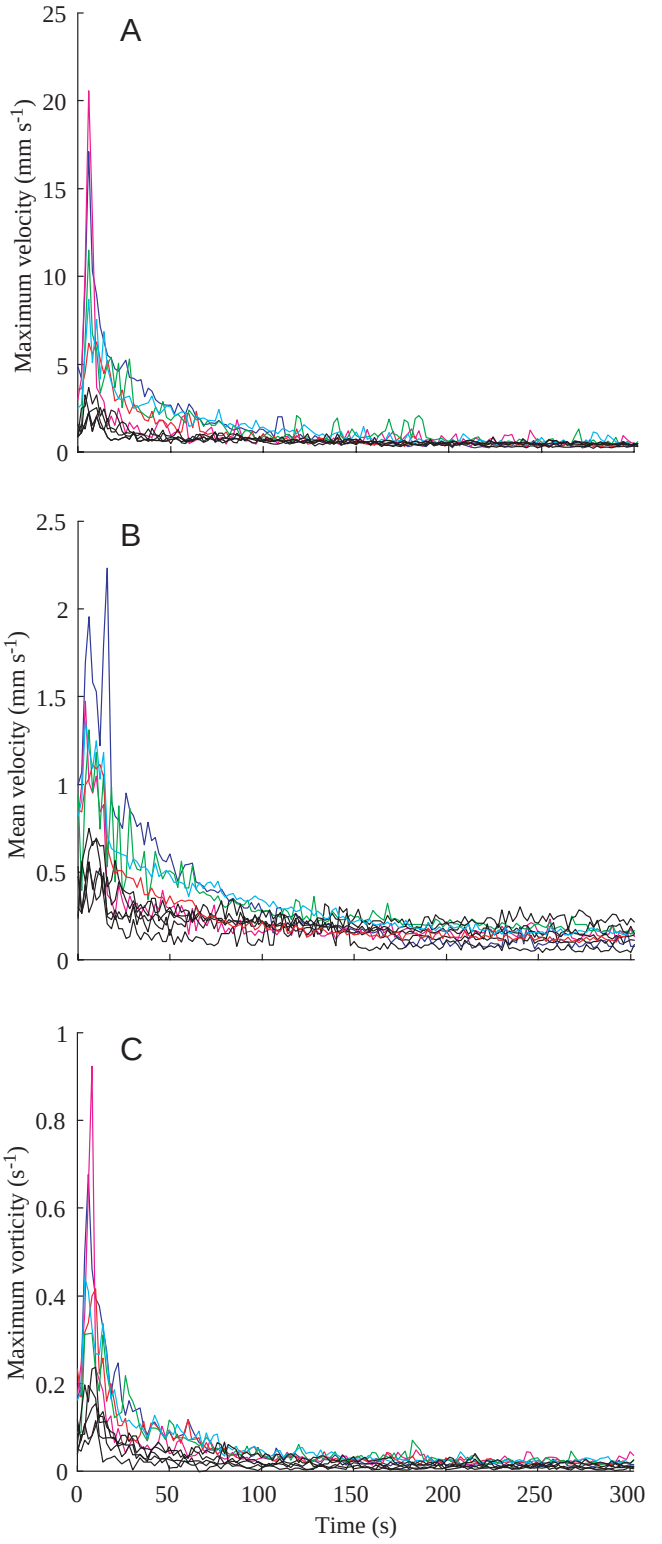

Fig. 2. Maximum velocity (A), mean velocity (B) and vorticity (C) as a function of time (t=0 s indicates the time when the fish entered the field of view) for five swimming trials each by a 6 cm (black lines) and a 10 cm (coloured lines) goldfish. The mean velocity values in Fig. 3B were obtained by averaging over the whole field of view (also listed in Table 1).

Table 1. *Characteristic features of fish-generated water disturbances for two different goldfish*

Trial	Body length (cm)	v_{max} (mm s^{-1})	v_{AVmax} (mm s^{-1})	v_{max300} (mm s^{-1})	v_{AV300} (mm s^{-1})	Relevant figure	t_{pass} (s)	Speed (cm s^{-1})			Description
								Minimum	Average	Maximum	
1	10	17	2.0	0.35	0.09	3A	4.9	5.4	8.1	14.1	Change of direction approximately 30 ° with a half tail flick
2	10	20	1.6	0.52	0.17	3B	5.2	5.5	7.1	9.0	Change of direction less than 10 °. Two half tail flicks followed by low-amplitude undulation
3	10	6	1.1	0.37	0.12	3C	2.4	10.0	14.6	19.0	Change of direction less than 10 °. Two full tail flicks
4	10	11	1.3	0.51	0.17	3D	4.0	7.8	10.4	13.8	Change of direction approximately 15 ° with tail flick to one side; low-amplitude undulation when leaving field of view
5	10	15	1.3	0.48	0.15	3E	3.9	6.0	8.4	11.6	Change of direction less than 10 °. Full tail flick in the middle of the field of view, followed by half tail flick when leaving
6	6	3	0.7	0.30	0.18	3F	2.8	5.9	9.0	13.4	Two changes of direction (20 ° followed by 30 °), each with a half tail flick
7	6	3.5	0.7	0.21	0.11	3G	2.3	7.9	11.0	13.0	Two changes of direction (30 ° followed by 12 °), each with a half tail flick
8	6	2.5	0.7	0.30	0.23	3H	2.1	8.0	9.7	14.0	Three slight changes of direction (15 °,20 °,10 °), two of them with a half tail flick, the last one with a full tail flick and an acceleration of approximately 40 %
9	6	2.2	0.4	0.32	0.06	3I	2.7	7.6	11.0	14.4	Two changes of direction (15 °,10 °, half tail flicks), followed by an additional tail flick without change of direction
10	6	2.2	0.6	0.32	0.13	3J	1.6	13.8	16.8	20.7	Multiple fast tail flicks, high swimming speed, straight swimming path (less than 5 ° change in direction)

Water velocity values represent minimum estimated values, see Materials and methods.

Analysis was performed as described in the legends to Figs 2 and 4.

v_{max}, maximum water velocity in the trial; v_{AVmax}, maximum of the spatial average of water velocity (averaged over the complete field of view); v_{max300}, maximum velocity found in the complete field of view after 300 s; v_{AV300}, average velocity after 300 s (averaged over the complete field of view); t_{pass}, duration of passage (from the time when the snout entered to the time when the tail left the field of view); speed, swimming speed of fish within field of view (minimum, average, maximum).

using a moving average validation algorithm (Host-Madsen and McCluskey, 1994).

Second, since the field of view was wide enough to cover the width of the wake, limited spatial resolution resulted in considerable velocity gradients within interrogation areas. Velocity gradients within an interrogation area bias the velocity measurement towards zero as a result of various effects (Keane and Adrian, 1992; Westerweel, 1997).

Third, the resolution of the smaller structures of the vortices was limited. Vorticity was calculated on the basis of a limited set of vectors using a linear approach (Landau and Lifshitz, 1966), which also biases the measured value towards zero (Lourenco and Krothapalli, 1995). Since all these error sources are effective in the same direction, our results give a lower boundary for the true values. This effect is greatest for the large velocity and vorticity values at the leading edge and can be assumed to fall below the noise level for the lowest measured values.

Results

Below, we present velocity profiles and dimensions for 10 wakes produced by the goldfish. Fig. 1 shows the water velocities as vector fields (left) and the corresponding vorticities as contour lines (right) in a typical example (trial 1) for t=0.6 s, 1.5 s, 2.3 s and 7.8 s where t=0 is the time when the snout of the fish enters the field of view. Vorticity, rot(v), is defined as:

$$\mathrm{rot}(v) = \left(\frac{\partial v_z}{\partial y} - \frac{\partial v_y}{\partial z}\right)\mathbf{e_x} + \left(\frac{\partial v_x}{\partial z} - \frac{\partial v_z}{\partial x}\right)\mathbf{e_y} + \left(\frac{\partial v_y}{\partial x} - \frac{\partial v_x}{\partial y}\right)\mathbf{e_z}, \quad (1)$$

where v is the velocity vector, x, y and z are Cartesian coordinates, and $\mathbf{e_i}$ are unit vectors in the respective direction. In a physical flow, a vorticity different from zero indicates a vortex. In the example shown in Fig. 1, the maximum velocity at 7.8 s exceeds 17 mm s^{-1}, and the mean velocity averaged over the field of view at 7.8 s exceeds 2 mm s^{-1}. These values represent low estimates of the true velocity (see Materials and methods). Table 1 shows the corresponding values for four additional passages of the 10 cm fish and five passages of the 6 cm fish.

Fig. 2A,B shows the development of the maximum and mean water velocity over time for the 10 trials; Fig. 2C shows the corresponding vorticity. Both the velocity and the vorticity reach a maximum when the fish is in the field of view. Fig. 3 describes the changes in velocity with time in the 10 trials, plus an additional wake from a coasting fish (Fig. 3K). In most of the examples, the range of high velocity moved laterally according to the moving vortices.

Comparison of the trajectory with a vortex ring model

The propagation trajectory of the water disturbances in trial 1 was compared with the propagation trajectories of laminar vortex rings studied by Saffman (1970) and Weigand and Gharib (1997). This comparison allows us to investigate further whether swimming goldfish produce a wake composed of laminar vortex rings. The vortex ring model is in accord with the observation that the vertical spread of fish-generated wakes was considerably less than its horizontal spread. This qualitative observation was made in trials in which the fish passed the field of view above or below the illuminated layer.

Saffman (1970) provides an equation for vortex rings with a small core size and a constant diameter and gives a relationship for the evolution of the propagation velocity of a vortex ring based on dimensional arguments. This relationship is appropriate for comparison with the present data, since it does not assume a small core size and allows the viscous length scale to be of the order of the vortex ring diameter, i.e. $t \approx 25D^2$ s cm^{-2}, where t is time and D is the diameter of the vortex ring. Its normalized form is:

$$U^*(t^*) = \frac{16\pi}{k}\,(1 + 16k't^*)^{-3/2}, \quad (2)$$

where U^* and t^* are normalized versions of propagation velocity and time, and k and k' are proportionality constants related to the impulse and to the viscous decay, respectively. Normalization of the propagation velocity U to U^* and the time t to t^* was performed using $U^*=2\pi DU/\Gamma$ and $t^*=\nu t/(4D^2)$, where D is the diameter of the vortex ring at t=0 s, Γ is the circulation of the vortex ring and ν is the kinematic viscosity of the fluid medium, here taken as 0.01 cm s^{-2}.

The distance S^* covered by a propagating vortex ring is obtained by integrating equation 2 and setting $S^*(0)$=0:

$$S^*(t^*) = \frac{-2\pi}{kk'}\,(1 + 16k't^*)^{-1/2} + \frac{2\pi}{kk'}. \quad (3)$$

Fig. 4 (circles) shows the propagation of the fish-generated water disturbance from trial 1, estimated from Fig. 3A (where the propagation path was nearly perpendicular to the swimming path), normalized as described in equations 2 and 3. For normalization, the vortex ring diameter was set to 3 cm, and the circulation was set to 5.3 cm^2 s^{-1}. The error involved in using these values will not affect the following discussion because of the normalization procedure. Line *a* in Fig. 4 is the best fit of equation 3 to these data, yielding k=15.9 and k'=11.5.

Weigand and Gharib (1997) presented measurements of the trajectories of laminar vortex rings with a diameter of 3 cm generated by a step-motor-driven piston. The Reynolds number $Re=\Gamma/\nu$ was between 830 and 1650, ν was assumed to be 0.01 cm^2 s^{-1}, the kinematic viscosity of water at 20 °C, and was measured using a laser Doppler anemometer. They found their data to be consistent with equation 2 with the best fit yielding k=14.4 and k'=7.8. All measured data were within the range of k=13.6, k'=7.5 (upper bound) to k=14.5, k'=10.6 (lower bound).

Lines *b*, *c* and *d* in Fig. 4 show plots of equation 3 with k=14.5, k'=10.6 (line *b*), k=14.4, k'=7.8 (line *c*) and k=13.6,

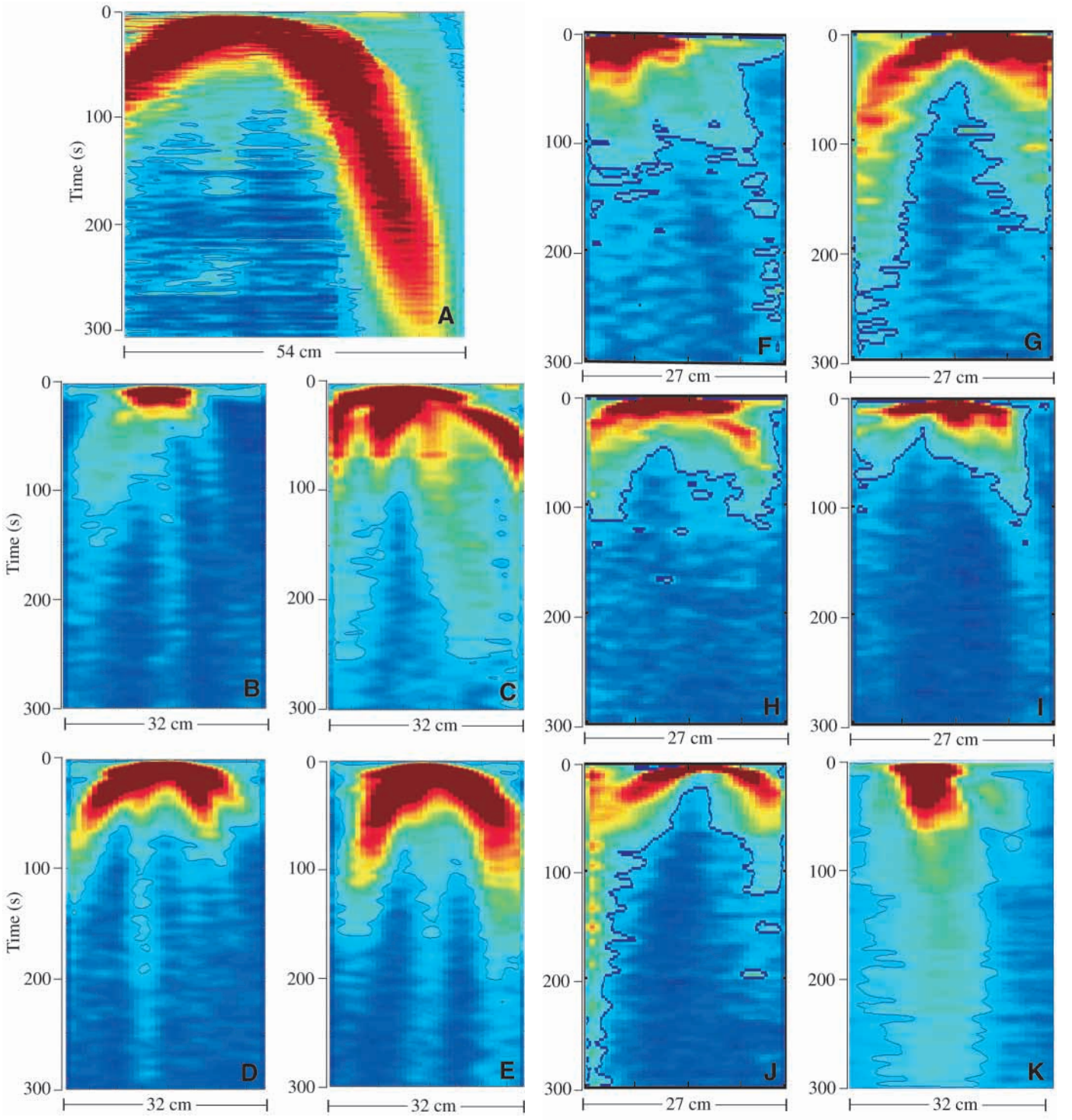

Fig. 3. (A–K) Water velocity as a function of time for 11 trials. Velocity is shown coded by colour, where red encodes the highest and dark blue the lowest water velocity. The blue contour line indicates a velocity of 0.2 mm s^{-1}, which can safely be assumed to exceed the sensitivity threshold of most lateral-line systems. Velocities were averaged over columns of each vector field to reduce each vector field to one row. The rows for subsequent points in time, separated by 1 s, were put together to visualize the time structure of the wake. Thus, the *y* axes in these figures are time axes running from 0 s, where the fish entered the field of view (top), to 300 s after passage. The fish left the field of view at t=1.6 s to t=5.2 s (see Table 1). For each trial except K, a short description of the fish movement is given in Table 1. A was constructed from the fields of view of two cameras and represents the whole width of the wake. K represents an example not given in Table 1 in which the fish coasted through the field of view while decelerating. A–E, K, 10 cm fish; F–J, 6 cm fish.

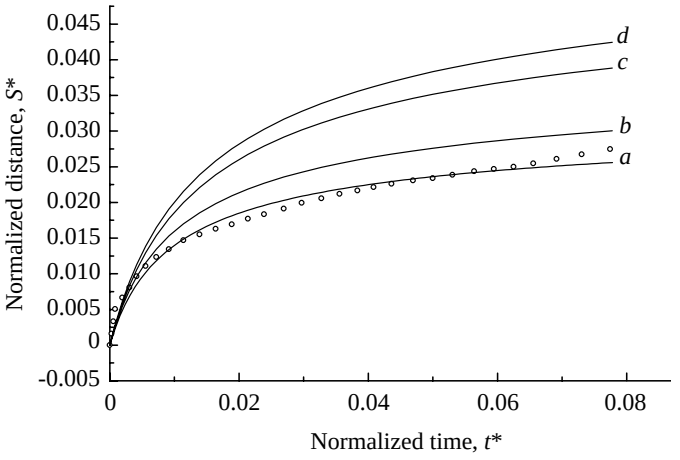

Fig. 4. Plot of the present data compared with the theory of Saffman (1970) and the experimental data of Weigand and Gharib (1997). The *x* axis shows the normalized time since the fish passed, $t^*=\nu t/(4D^2)$, where $t^*=0$ s is the time when the fish entered the camera field. The *y* axis shows the normalized distance covered by the water disturbance lateral to the swimming path or the distance between the vortex ring and the vortex ring generator. The normalized distance covered is $S^*=S[(\pi\nu/2D\Gamma)]$. For further explanation, see text. *t* is the time since the fish entered the field of view, *S* is the distance covered, ν is kinematic viscosity, *D* is the diameter of the vortex ring at $t=0$ s. Open circles, lateral spread of water disturbance in trial 1 (see Table 1; Fig. 3A); line *a*, best fit of equation 3 to the data from trial 1 (k=15.9, k'=11.5); lines *b*, *d*, upper and lower bound for the experimental results of Weigand and Gharib (1997); line *c*, best fit of equation 3 to the experimental data of Weigand and Gharib (1997) (k=14.4, k'=7.8). k and k' are proportionality constants related to the impulse and to the viscous decay, respectively.

k'=7.5 (line *d*); i.e. the upper and lower bounds and the best fit to the experimental data of Weigand and Gharib (1997). As can be seen, the fish-generated water disturbance in the present study spread considerably less far than the laminar vortices produced by a step-motor-driven piston (Weigand and Gharib, 1997). However, equation 3 derived from the propagation velocity of a laminar vortex trajectory fitted our data well (note that the gradient of line *a* is shallower than our data above t^*=0.03).

Discussion

Our measurements show that a small swimming fish leaves a hydrodynamic trail in the water that potentially could inform other animals, such as predators, about its presence even several minutes after its passage. Even after this period, the trails contain information about the direction in which the fish has moved and the time that has passed since it swam by. The latter is indicated by the decay of vorticity in the vortex street. Vorticity cannot be measured directly, but must be derived from multiple point velocity measurements. However, some fish, including goldfish, have up to several hundred superficial neuromasts on each side of the body (e.g. Puzdrowski, 1989). Thus, in principle, their lateral line should be able to make simultaneous velocity measurements at multiple points, an important prerequisite for the estimation of the vorticity in a fish-generated wake.

The swimming direction of a fish can be derived from the velocity gradient in its wake and, at least when a fish is gliding, from the direction of gross water flow in the wake (see Fig. 1), which will persist for more than 60 s. The width of a track and the amount of water velocity depend on the body size of the track generator, i.e. the size of a potential prey object (Table 1; Fig. 3).

A comparison of our data with the theoretical model of Saffman (1970) and the experimental data of Weigand and Gharib (1997) provides further evidence that fish-generated water disturbances partially propagate as vortex-ring-like structures. Compared with the data of Weigand and Gharib (1997), the fish-generated vortices had a lower propagation distance. This may partly be due to turbulent regions in fish-generated vortices (Bleckmann et al., 1991). In addition, interaction between the vortices in the vortex street will pull the vortices towards the middle of the street. These effects could not be quantified in our analysis. The shape of the cross section of a laminar vortex ring will influence its propagation behaviour (e.g. Shariff and Leonard, 1992). The proportionality constant k should range between zero for a Rankine vortex with small core size and 16 for a spherical Hill's (Hill, 1894) vortex. The value of k=15.9 obtained from the best fit to our data (see Fig. 4) therefore indicates that fish-generated vortices have a horizontal cross section that is more similar to a Rankine vortex (Blickhan, 1992, 1997; Müller et al., 1997) than to a Hill's vortex. Thus, we can obtain an idea of the three-dimensional structure of the wake which could not be measured directly using our two-dimensional PIV device.

It has never been demonstrated conclusively that fish use hydrodynamic wakes when hunting prey. However, blindfolded seals can track the hydrodynamic wake caused by a model submarine (G. Dehnhardt and B. Mauck, unpublished data), suggesting that seals might be able to hunt fish by following their vortex trails. Behavioural experiments are under way in our laboratory to investigate this further. Lateral line thresholds are 2–3 orders of magnitude more sensitive than the hydrodynamic thresholds of seals (e.g. Bleckmann, 1994; Dehnhardt et al., 1998). In addition, fish can discriminate not only between water motions that differ in frequency, amplitude or frequency modulation (Bleckmann, 1994) but also between those caused by moving objects that differ in size, shape or speed and direction of movement (D. Vogel and H. Bleckmann, unpublished data). Thus, the lateral line of fish could potentially detect and analyze fish-produced vortex trails such as those recorded here.

We thank Dr Joachim Mogdans for helpful comments on the manuscript, Hüls AG (Marl) for donating the neutrally buoyant particles and Dr Denise R. McCluskey for supplying literature on the validation of PIV measurements obtained under non-ideal conditions. The research reported herein was

performed under the guidelines established by the current German animal protection law ('Tierschutzgesetz').

References

Adrian, R. J. (1991). Particle-imaging techniques for experimental fluid mechanics. *Annu. Rev. Fluid Mech.* **23**, 261–304.

Adrian, R. J. (1997). Dynamic ranges of velocity and spatial resolution of particle image velocimetry. *Meas. Sci. Techn.* **8**, 1392–1399.

Bleckmann, H. (1994). Reception of hydrodynamic stimuli in aquatic and semiaquatic animals. In *Progress in Zoology*, vol. 6 (ed. W. Rathmayer), pp. 1–115. Stuttgart, Jena, New York: Gustav Fischer Verlag.

Bleckmann, H., Breithaupt, T., Blickhan, R. and Tautz, J. (1991). The time course and frequency content of hydrodynamic events caused by moving fish, frogs and crustaceans. *J. Comp. Physiol.* A **168**, 749–757.

Blickhan, R. (1992). Biomechanik der axialen aquatischen und der pedalen terrestrischen Lokomotion. Habilitationsschrift, University of Saarland, Saarbruecken, Germany.

Blickhan, R. (1997). Hydrodynamik der undulatorischen Lokomotion. *Biona-Report* **11**, 331–351.

Blickhan, R., Krick, C., Breithaupt, T., Zehren, D. and Nachtigall, W. (1992). Generation of a vortex-chain in the wake of a subundulatory swimmer. *Naturwissenschaften* **79**, 220–221.

Blickhan, R., Krick, C. and Nachtigall, W. (1990). Flow in the vicinity of swimming fish. In *Verhandlungen der Deutschen Zoologischen Gesellschaft*, no. 80 (ed. H.-D. Pfannenstiel), p. 630. Stuttgart: Gustav Fischer Verlag.

Budelmann, B.-U. and Bleckmann, H. (1988). A lateral line analogue in cephalopods: water waves generate microphonic potentials in the epidermal head lines of *Sepia* and *Lolliguncula*. *J. Comp. Physiol.* A **163**, 1–5.

Coombs, S., Fay, R. R. and Janssen, J. (1989). Hot-film anemometry for measuring lateral line stimuli. *J. Acoust. Soc. Am.* **85**, 2185–2193.

Coombs, S. and Janssen, J. (1989). Peripheral processing by the lateral line system of the mottled sculpin (*Cottus bairdi*). In *The Mechanosensory Lateral Line. Neurobiology and Evolution* (ed. S. Coombs, P. Görner and H. Münz), pp. 299–319. New York: Springer-Verlag.

Dehnhardt, G., Mauck, B. and Bleckmann, H. (1998). Harbour seals detect minute water movements by means of their whiskers. *Nature* **394**, 235–236.

Freek, C., Sousa, J. M. M., Hentschel, W. and Merzkirch, W. (1997). Digital image compression PIV – a tool for IC engine research. *Proc. Int. Symp. Laser Anem. Adv. Appl.* **7**, 455–464.

Görner, P. (1963). Untersuchungen zur Morphologie und Elektrophysiologie des Seitenlinienorgans vom Krallenfrosch (*Xenopus laevis* Daudin). *J. Comp. Physiol.* A **47**, 316–338.

Hanke, W. and Bleckmann, H. (1997). Flow visualization and particle image velocimetry with a custom made inexpensive device. In *Verhandlungen der Deutschen Zoologischen Gesellschaft*, no. 92 (ed. D. Zissler), p. 352. Stuttgart: Gustav Fischer Verlag.

Hanke, W. and Brücker, C. (1998). The time course of a goldfish's vortex street measured and analyzed with a custom made PIV device. *Fachtagungen der Deutschen Gesellschaft für Laseranemometrie GALA e. V.* **6**, 51–57.

Hill, M. J. M. (1894). On a spherical vortex. *Phil. Trans. R. Soc. Lond. A* **185**, 213–245.

Host-Madsen, A. and McCluskey, D. (1994). On the accuracy and reliability of PIV measurements. *Seventh International Symposium on the Application of Laser Techniques to Fluid Mechanics*, 1–11. Lisbon.

Keane, R. D. and Adrian, R. J. (1992). Theory of cross-correlation analysis of PIV images. *Appl. Sci. Res.* **49**, 191–215.

Kirk, K. L. (1985). Water flows produced by *Daphnia* and *Diaptomus*: Implications for prey selection by mechanosensory predators. *Limnol. Oceanogr.* **30**, 679–686.

Krick, C., Blickhan, R. and Nachtigall, W. (1997). Architektur und Energetik der Wirbelstrasse frei schwimmender Fische. In *Verhandlungen der Deutschen Zoologischen Gesellschaft*, no. 91 (ed. H.-D. Pfannenstiel), p. 101. Stuttgart, Jena, New York: Gustav Fischer Verlag.

Landau, L. D. and Lifschitz, E. M. (1966). *Lehrbuch der theoretischen Physik, Band VI: Hydrodynamik*. Berlin: Akademie-Verlag.

Lourenco, L. and Krothapalli, A. (1995). On the accuracy of velocity and vorticity measurements with PIV. *Exp. Fluids* **18**, 421–428.

McCutchen, C. W. (1977). Froude propulsive efficiency of a small fish, measured by wake visualization. In *Scale Effects in Animal Locomotion* (ed. T. J. Pedley), pp. 339–363. London, New York, San Francisco: Academic Press.

Merzkirch, W. (1987). *Flow Visualization*. New York: Academic Press. 260pp.

Müller, U. K., van den Heuvel, B. L. E., Stamhuis, E. J. and Videler, J. J. (1997). Fish foot prints: morphology and energetics of the wake behind a continuously swimming mullet (*Chelon labrosus* Risso). *J. Exp. Biol.* **200**, 2893–2906.

Puzdrowski, R. L. (1989). Peripheral distribution and central projections of the lateral-line nerves in goldfish, *Carassius auratus*. *Brain Behav. Evol.* **34**, 110–131.

Rosen, M. W. (1959). *Water Flow About a Swimming Fish.* US Naval Ordnance Test Station TP 2298, China Lake, California, USA. 96pp.

Saffman, P. G. (1970). The velocity of viscous vortex rings. *Stud. Appl. Math.* **49**, 371–380.

Shariff, K. and Leonard, A. (1992). Vortex rings. *Annu. Rev. Fluid Mech.* **24**, 235–279.

Stamhuis, E. J. and Videler, J. J. (1995). Quantitative flow analysis around aquatic animals using laser sheet particle image velocimetry. *J. Exp. Biol.* **198**, 283–294.

Tautz, J. and Sandeman, D. (1980). The detection of water borne vibration by sensory hairs on the chelae of the crayfish. *J. Exp. Biol.* **88**, 351–356.

Vogel, S. and Feder, N. (1966). Visualization of low-speed flow using suspended plastic particles. *Nature* **203**, 186–187.

Weigand, A. and Gharib, M. (1997). On the evolution of laminar vortex rings. *Exp. Fluids* **22**, 447–457.

Westerweel, J. (1997). Fundamentals of digital particle image velocimetry. *Meas. Sci. Techn.* **8**, 1379–1392.